Finite Element Simulation of Complex Jets in a Crossflow for V/STOL Applications

Tae S. Oh* and Joseph A. Schetz†
Virginia Polytechnic Institute and State University, Blacksburg, Virginia 24061

The paper presents a prediction method for the flowfield and surface pressure distribution induced by three-dimensional jets injected from a flat surface into a crossflow. An eddy viscosity model extended from Prandtl's concept has been developed to account for the curved nature of the jets with arbitrary cross-sectional shape. The first-order influence of the fluctuating nature of the turbulent flow is reflected via axial turbulence information. The Reynolds-averaged, Navier-Stokes equations are solved using the finite-element method, and the penalty function method is used to discretize the pressure in a consistent manner. The eight-noded, isoparametric finite element is used to approximate the computational domain and the field variables. The performance of the present prediction method is verified for a single circular jet in a crossflow at $R = 4$, which has enough measured data available for detailed comparisons. The jet trajectory and axial velocity decay comparison are excellent, and the surface pressure distribution is well predicted except for the wake region right behind the jet. The same methodology is then applied to single- and dual-rectangular jets in a crossflow at the same velocity ratio, and most of the important features of the surface pressure distribution are predicted well. The general observation is that the entrainment process due to the turbulent mixing is modeled reasonably through a generalized eddy viscosity concept supported by an axial turbulence intensity correlation, and the agreement achieved here between the prediction and existing measured data is considered good for a three-dimensional, turbulent flow of this complexity.

Nomenclature

a	= constant, = 1/.53
b	= shear layer width
$b_{1/2}$	= averaged jet half width
C	= constant
C_p	= pressure coefficient
D	= diameter, $= D_j = D_{eq}$
f	= proportionality factor for eddy viscosity
f_i	= vector of body forces
L	= streamwise length of the rectangular nozzle
L_{pc}	= length of the potential core
n	= direction normal to the boundary
P	= static pressure
q	= dynamic pressure
R	= jet-to-crossflow velocity ratio
t_i	= vector of surface traction
U, V, W, or U_i	= mean velocity components
U_{max}	= maximum velocity
U_c	= axial velocity
u', v', w'	= fluctuating velocity components
$-\rho\overline{u'v'}$	= Reynolds shear stress in xy plane
x, y, z, or x_i	= Cartesian coordinates
α	= angle between the jet axis and x axis
Γ	= boundary of the computation domain
δ	= variational symbol
δ_{ij}	= Kronecker delta
ϵ	= penalty parameter
μ_T	= eddy viscosity
ν_T	= kinematic eddy viscosity
Ω	= bounded computation domain
φ	= element interpolation function for velocity
ρ	= density of the fluid
ψ	= element interpolation function for pressure
ξ, ζ, η	= intrinsic coordinates
$[c]$	= element gradient matrix
$\{f\}$	= element force vector
$\{F\}$	= global force vector matrix
$[k]$	= element stiffness
$[K]$	= global stiffness matrix
$[m]$	= element pressure mass matrix
$\{p\}$	= nodal pressure vector in an element
$\{u\}$	= nodal velocity vector in an element
$\{U\}$	= column vector of velocity unknown

Introduction

JETS injected into a crossflow have been widely studied due to their large area of engineering applications. A general description of these flows can be found in Schetz[1] and Abramovich.[2] There have been numerous experimental works[3-7] that have tried to reveal some of the fundamental transport mechanisms and mixing processes. As for the computational studies, the use of the full Navier-Stokes equations on this problem was first reported in Chien and Schetz.[8] A two-equation turbulence model was used in Patankar et al.[9] and White,[10] a high resolution of the vorticity field was visualized with a turbulent kinetic energy (TKE) model in Sykes et al.,[11] and recently, a finite element solution of the parabolized model was reported in Baker et al.[12] Also, a three-dimensional elliptic code using a standard k-ϵ turbulence model has been widely employed in combustion modeling[13,14] for gas turbine

Presented as Paper 88-3269 at the AIAA/ASME/SAE/ASEE 24th Joint Propulsion Conference, Boston, MA, July 11-13, 1988; received July 21, 1988; revision received Oct. 20, 1989.

*Graduate Research Assistant, Aerospace and Ocean Engineering Department; currently Senior Researcher, Aerospace R&D Center, Samsung Aerospace Industries, Ltd., Seoul, Korea. Member AIAA.

†W. Martin Johnson Professor and Department Head, Aerospace and Ocean Engineering Department Fellow AIAA.

applications. But, the prediction of surface pressure, which is of prime importance for V/STOL applications, has been hardly reported in these studies. Instead, only inviscid flow methods supported by empirically tuned jet properties have been the major prior technique to predict the body pressure distribution.[15] Though these methods offer the advantage that the desired body pressure distribution can be obtained without solving for the flowfield throughout the domain, their range of application is limited to already known cases. This work is aimed at the development of a robust, viscous prediction method for the pressure and mean flowfield with the aid of the least possible amount of empirical information.

The surface pressure induced by the jet flow characterizes the aerodynamic performance of a V/STOL aircraft in transition from hover flight to wingborne operation and vice versa at a fairly low speed. Recent experimental studies in this area include various parameters: rectangular nozzles,[7,19,20] dual jet configurations,[7,16,17,18,19] nonuniformity of the jet exit conditions,[7,18,21,22] and injection from a body of revolution,[16,23] among others. Streamwise aligned rectangular jets have received special attention due to the convenience of installation of dual nozzles on the side of V/STOL aircraft and less blockage effect against the crossflow for the same jet exit area.

The surface pressure is characterized by the mass entrainment of the crossflow into the jet, and this mechanism in the near field of the jet at high R is believed to be similar to that for the initial region of the two-dimensional jets. This motivated the development of the current turbulent model, which obtains the length and velocity scales not from empirical correlations but from the flowfield, which enables easy treatment of an arbitrarily shaped jet cross section.

Using the Bousinesq approximation, the momentum and continuity equations are discretized and solved by the penalty function finite element method, in which the pressure is eliminated at the elemental level and the final system of algebraic equations can be solved for velocity components only. Also, Gaussian elimination does not require partial pivoting, which makes it attractive to apply the direct profile method, even in three dimensions. Special boundary conditions are employed to perform computations in a computational region of limited size with a modest mesh, and these are found to be effective for simulating the main jet flowfield at R in the range of 4, which is important for V/STOL and other practical applications.

Three different nozzle configurations are considered in this study: a single circular nozzle, a single streamwise aligned rectangular (aspect ratio 4) nozzle, and dual rectangular nozzles. The present turbulence model and numerical strategies are tested on the first problem, which has ample experimental data. The second and third cases involve newer issues with practical importance, and the computed results are compared to some recent experiments.[7,19]

Analysis

Governing Equations

The incompressibility and the Reynolds-averaged, Navier-Stokes equations in the steady-state are given by

$$U_{i,i} = 0 \tag{1}$$

$$\rho U_j U_{i,j} = \sigma_{ij,j} + \rho f_i \tag{2}$$

where $\sigma_{ij} = -P\delta_{ij} + \tau_{ij}$ and $\tau_{ij} = (\mu + \mu_T)(U_{i,j} + U_{j,i})$, and the pressure was redefined to include the effects of the turbulent normal stresses.

Variational and Finite Element Formulations

Full details of the mathematical procedures associated with the penalty function finite element methods are readily available,[24-27] so only a brief outline is given here. The variational (weak) form for the Navier-Stokes equations can be obtained by using a Generalized Galerkin technique. Indeed, this is one of the methods of weighted residuals that seeks a linearly independent set of weighting functions orthogonal to the residual by making the integral of the weighted residual become zero. Taking the variation of velocity and pressure as δU_i and δP, respectively, and using a penalty approximation for pressure as $U_{i,i} = -\epsilon P$, the weak forms can be given as

$$\int_\Omega (\delta U_i \rho U_j U_{i,j} - \delta U_{i,j} P + \delta U_{i,j}\tau_{ij} - \delta U_i \rho f_i)\mathrm{d}\Omega = \oint_\Gamma \delta U_i t_i \mathrm{d}\Gamma \tag{3}$$

$$\int_\Omega \delta P U_{i,i}\mathrm{d}\Omega = -\epsilon \int_\Omega (\delta P) P \mathrm{d}\Omega \tag{4}$$

where $t_i = \sigma_{ij}n_j$ represents the applied surface stress in the i direction. Within each element, the velocity and pressure are approximated via interpolation functions $\{\varphi\}$ and $\{\psi\}$ defined as

$$U_i = \{\varphi\}^T\{u\} = \sum_k \varphi_k U_{i,k} \tag{5}$$

$$P = \{\psi\}^T\{p\} = \sum_k \psi_k P_k \tag{6}$$

where $\{u\}$ and $\{p\}$ represent the vector of nodal values of velocity components and pressure, respectively. Evaluating integrals over the element, the finite element equations for momentum and continuity equations are given in a compact matrix-vector form as

$$[k]\{u\} - [c]\{p\} = \{f\} \tag{7}$$

$$[m]\{p\} = (-1/\epsilon)[c]^T\{u\} \tag{8}$$

Here, $\{f\}$ means the elemental force vector at the nodal points. Eliminating the pressure in Eq. (7) using Eq. (8), the final form may be given as

$$([k] + (1/\epsilon)[c][m]^{-1}[c]^T)\{u\} = \{f\} \tag{9}$$

It should be noted that the pressure degrees of freedom are eliminated at the elemental level and the only unknowns are velocity components, which result in tremendous computational savings, especially in three-dimensional cases. This consistent construction of the penalty matrix evaluated with full quadrature is known to be more accurate than the reduced integration counterpart when distorted elements are employed.[24,25] Convergence of the solution of the penalty formulation to the true solution, as $\epsilon \to 0$, can be proved.[26] A value of ϵ of 10^{-5}-10^{-9} is used according to the magnitude of the viscosity. Once the velocity field is obtained, the pressure is recovered via

$$P = (-1/\epsilon)U_{i,i} \tag{10}$$

Turbulence Model

The choice of the turbulence model for the calculation of a jet in a crossflow has been controversial.[28] Further, the previous elliptic approaches with two-equation turbulence models[9,10,13,14] indicated grid dependence of the solutions, and it has never been clear whether the discrepancy of the prediction compared to experiment should be attributed to numerical diffusion or inadequacy of the turbulence model. According to recent studies,[28,29] the effect of the turbulence model should be small, and a crude eddy-viscosity model may be employed for high R[30], even though it may not be valid throughout the entire flowfield. This is a partial justification of the choice of the present rather simple turbulence model. The proposed turbulence model does not presume or require assumed profile shape in any coordinate direction. The main idea is to describe the curved jet with respect to the jet trajectory and quantify

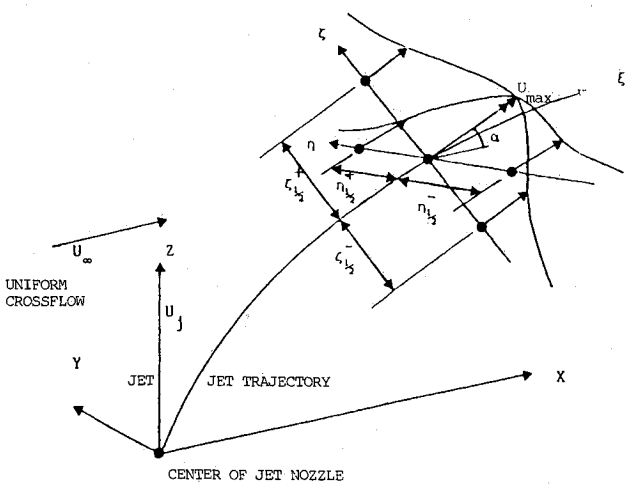

Fig. 1 Definition sketch of the velocity profile of a jet in crossflow.

the characteristic length and velocity scales to determine the levels of turbulence transport. We propose to use an eddy-viscosity model, whose functional form is simply a product of length and velocity scales, which are assumed to be constant across the jet.

A sketch of the jet for analysis in Cartesian and intrinsic coordinate system is given in Fig. 1 along with definition of the various half width in each direction. Here, the jet trajectory or axis is defined as the locus of maximum total velocity in the plane of symmetry, and the jet half width is defined as the distance along ζ or η direction from jet axis to the location where ξ component of the local velocity satisfies the following relation:[31]

$$(U_\xi - U_\infty)/(U_{\max} - U_\infty) = 1/2 \tag{11}$$

Because the profile across the jet is asymmetric in general, the jet width is decomposed in both positive and negative directions with respect to the jet axis. The characteristic length scale here is defined as the jet half width in an averaged sense, and a convenient expression can be obtained by generalizing the three-dimensional, rectangular, free jet model suggested by Sforza et al.[32] including here the effect of the jet deflection as

$$b_{1/2}(\xi) = [\zeta^a_{1/2}\eta^a_{1/2}/(\zeta^a_{1/2} + \eta^a_{1/2})]^{1/a} \tag{12}$$

where

$$\zeta_{1/2} = (\zeta^-_{1/2} + \zeta^+_{1/2})/2 = (x^-_{1/2} + x^+_{1/2})\sin\alpha/2 \tag{13}$$

and

$$\eta_{1/2} = (\eta^-_{1/2} + \eta^+_{1/2})/2 = (y^-_{1/2} + y^+_{1/2})/2 \tag{14}$$

where α is the angle between the x axis and the jet axis, and $1/a = 0.53$.

Near the nozzle exit, there exists a potential core region where the turbulent mixing is not so active. In the present study, a linear relation for the coflowing planar jet given by Abramovich[2] is used to determine the growth of the mixing layer in this region as

$$db_{pc}/d\xi = (0.027/2)[(1 - 1/R)/(1 + 1/R)] \tag{15}$$

Integrating Eq. (15) from the nozzle exit gives

$$b_{pc} = (0.027/2)[(1 - 1/R)/(1 + 1/R)]\xi + b_{pc}(0) \tag{16}$$

where $b_{pc}(0)$ may be taken as the displacement thickness of the boundary layer at the nozzle exit. Introduction of this constant is for numerical reason to avoid a zero length scale in this region. The length b_{pc} can only be used as a reference length scale until it becomes greater than or equal to $b_{1/2}$. The resulting core length for $R = 4$ is about 3 jet diam, which is in good agreement with the estimation of Kamotani and Greber[4] or measured data of Pratte and Baines.[33] In the rectangular jet problem, there exist three distinctive regions[32]: potential core, characteristic decay, and axisymmetric decay region. Thus, the final choice of the length scale can be performed according to the logical sequence given in Fig. 2.

The velocity scale is taken here as the difference between the maximum total velocity and the freestream velocity, even though other choices are possible, as

$$\Delta U_c = U_{\max} - U_\infty \tag{17}$$

Then, the eddy viscosity can be given as

$$\mu_T = 0.037\rho b_{1/2}\Delta U_c \tag{18}$$

Here, the coefficient of 0.037 is taken, as described in Ref. 32, since this model can cover various two-dimensional coflowing jets in extreme cases and three-dimensional rectangular free jets.

Even though the expression above is developed for the jet of arbitrary cross-sectional shape, it must be viewed as a mean flow model that does not directly reflect the fluctuating nature of the turbulent flow. The eddy-viscosity models that have been successfully applied to jet or wake cases often do not perform adequately when applied to the other case, and this is so even when the functional forms of both kinds of models are essentially identical.[1] The primary controlling factor for this discrepancy is believed to be the proportionality constant, and there has been a study to investigate the connection between this constant and turbulence quantities through an order-of-magnitude analysis.[34] (See the Appendix for more details.) According to the results of this study, the same eddy-viscosity model can be applied to both jet and wake flows by adjusting

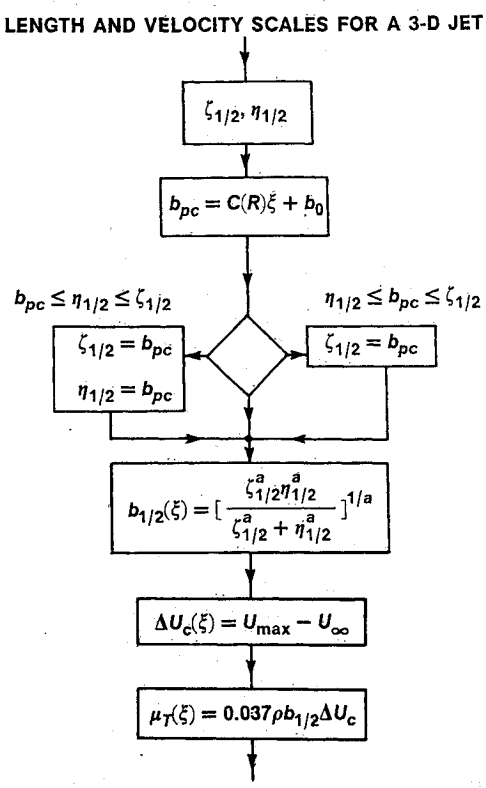

Fig. 2 Flow diagram for determination of the characteristic length hand velocity scales for the eddy-viscosity model.

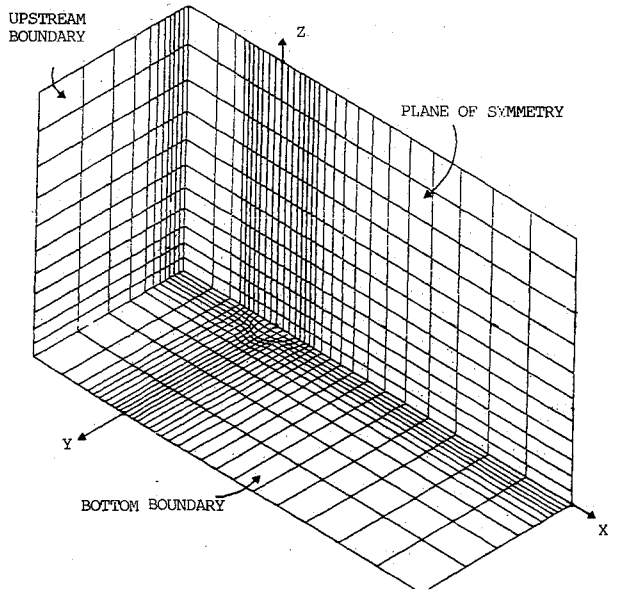

Fig. 3 Finite-element mesh for the single circular jet case.

the factor with the aid of axial turbulence intensity data. This algebraic turbulence function approach is introduced here to reflect the first-order influence of turbulence structure into an eddy-viscosity model for a curved jet. Let f be a function of the arc length of the jet that represents a relative magnitude of the axial turbulence intensity to the velocity defect:

$$f(\xi) = \overline{u'^2}/\Delta U_c^2 \tag{19}$$

and f can be correlated from the measured data of Keffer and Baines[3] as

$$f = \begin{cases} 2 & \text{in the potential core} \\ 1 + \exp[-1.134(\xi - \xi_0)] & \text{in the main jet region} \end{cases} \tag{20}$$

The final form of the eddy-viscosity model adopted here is given by

$$\mu_T = 0.037 f \rho b_{1/2} \Delta U_c \tag{21}$$

Nondimensionalization

Let L_0, U_0, and $\rho_0 U_0^2$ denote the characteristic reference magnitudes, and the asterisked dimensionless variables may be expressed as

$$x_i^* = x_i/L_0, \qquad i = 1,2,3 \tag{22}$$

$$U_i^* = U_i/U_0, \qquad i = 1,2,3 \tag{23}$$

$$P^* = (P - P_0)/\rho_0 U_0^2 \tag{24}$$

$$\rho^* = \rho/\rho_0 = 1 \tag{25}$$

Domain and Mesh

Because the flow is symmetric with respect to the xz plane passing through the jet nozzle, only half of the flowfield is considered for single jet cases. For the dual jet case, the center of the nozzle spacing served as the plane of the flow symmetry. All the origins of the reference frame are taken at the center of the jet nozzle, and the whole computation domain comprises a rectangular box shape. To determine the size of the domain and finite element mesh, a series of the pseudo-laminar calculations was performed[27] with repeated mesh refinement and domain adjustment within the computational resources available. At this stage, the eddy viscosity was set to a constant, and the round jet model used in Ref. 8 was selected for parametric study, in favor of cost effectiveness. With the final selected domain and mesh, the initial flowfield was obtained to drive the current turbulent model. A typical example of the finite element mesh is given for the single circular jet case in Fig. 3.

Boundary Conditions

After careful review of various choices, the following set of boundary conditions were used for all cases:

Upstream at $x^* = X_u$:

$$U^* = 1, \; V^* = W^* = 0 \tag{26}$$

Downstream at $x^* = X_d$:

$$t_x^* = t_y^* = t_z^* = 0 \tag{27}$$

Bottom boundary at $z^* = 0$:

Bottom wall except for the nozzle:

$$t_x^* = t_y^* = W^* = 0 \tag{28a}$$

Nozzle exit:

$$U^* = V^* = 0, \; W^* = R \tag{28b}$$

Nozzle edge:

$$U^* = V^* = W^* = 0 \tag{28c}$$

Top boundary at $z^* = Z$:

$$t_x^* = t_y^* = t_z^* = 0 \tag{29}$$

Plane of symmetry at $y^* = 0$:

$$t_x^* = V^* = t_z^* = 0 \tag{30}$$

Side boundary at $y^* = Y$:

$$t_x^* = t_y^* = t_z^* = 0 \tag{31}$$

The downstream boundary is regarded as an outflow boundary, and the traction-free condition is employed. The far-field boundaries are not so far from the injection nozzle as to specify either uniform freestream velocity[9] or zero normal velocity and zero tangential velocity gradients.[10,11] Physically, these surfaces should allow flow through the boundary, and

Table 1 Summary of computational information

Nozzle configuration	Single circular	Single rectangular	Dual rectangular
Ref. length	D	L	L
Location of the boundary			
Upstream (X_u)	−2.5	−1.5	−1.5
Downstream (X_d)	8.0	3.0	3.0
Side boundary (Y)	4.0	2.5	2.0
Top boundary (Z)	6.0	2.0	3.0
Finite element mesh	30×12×12	25×15×12	30×20×15
No. of nodal points	4,320	4,500	9,000
No. of elements	3,509	3,696	7,714
No. of active eqs.	11,807	12,267	24,975
No. of matrix elements	10,144,411	13,117,355	43,825,147
Mean half bandwidth	430	535	877
CPU s/1LU decomp.	197	292	6,673

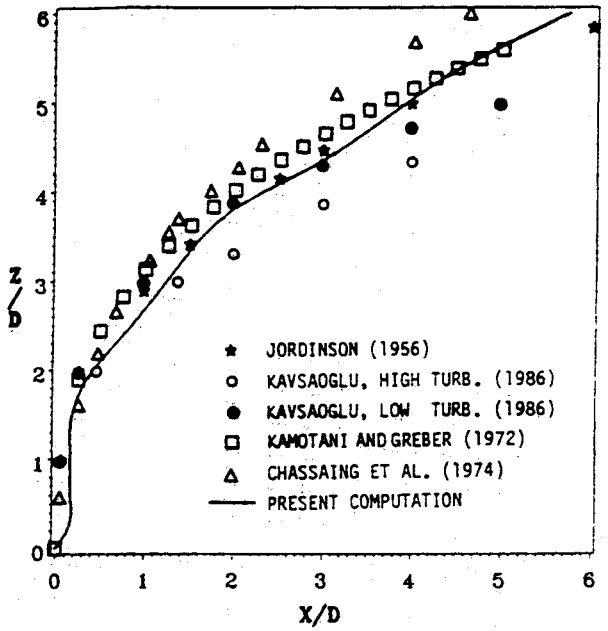

Fig. 4a Comparison of jet trajectory.

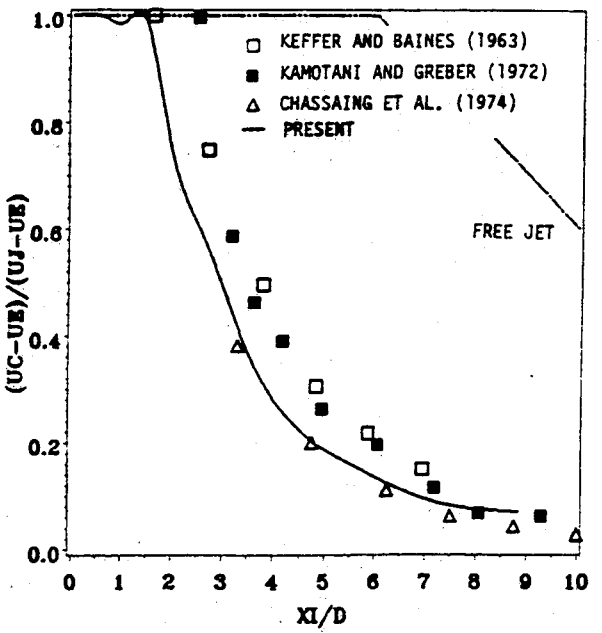

Fig. 4c Comparison of axial velocity decay.

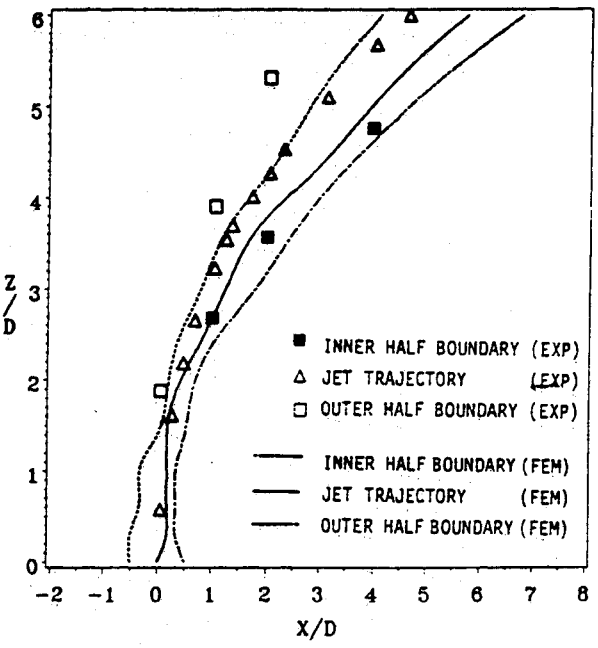

Fig. 4b Comparison of jet boundaries.

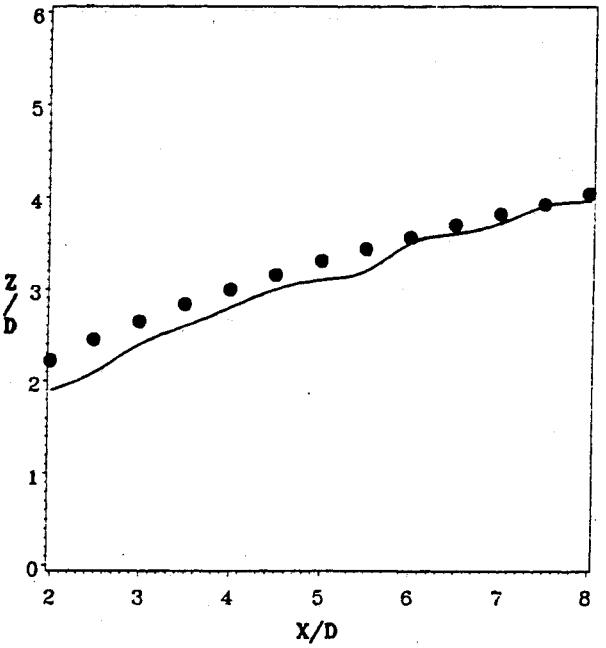

Fig. 4d Comparison of vortex curve.

the specification of the traction-free conditions was found to be more effective. The bottom wall is modeled as a stress-free wall that is similar to that used in Ref. 11. This approach may not give an accurate picture of the boundary layer flow but may be a useful approximation when the details of the boundary layer are not the major concern.[36]

Solution Strategy

To minimize the workspace, an eight-noded, isoparametric, trilinear, velocity-constant pressure element was employed. Though this element does not satisfy the Brezzi-Babuska condition[24] and may sometimes suffer from spurious pressure modes, these can be all filterable, at least when pure, on a regular mesh.[24,25] The pressure is computed only at the centroid point, which achieved filtered pressure. No other pressure mode was observed in the present computation.

Upon assembling Eq. (9) over the entire elements and imposing boundary conditions, the final matrix equations can be given as

$$[K(U)]\{U\} = \{F\} \tag{32}$$

where $[K(U)]$ is the global stiffness matrix, $\{U\}$ the global unknown vector, and $\{F\}$ the global vector of the body force and boundary conditions. Because of the steep velocity gradient near the jet nozzle, direct iteration (successive substitution) with under-relaxation was used starting from the pseudolaminar solution. The eddy-viscosity distribution along the jet axis is updated at every iteration using the current solution. The system matrix has a very large, unsymmetric, sparse, skylined-structure, but pivoting is not necessary for LU decomposition, and direct application of the profile solver is possible. Computations were performed using a modified version of the finite element method (FEM) code fluid dynamic analysis program (FIDAP)[37] on the Virginia Tech IBM 3090 machine with vector facility. Summarized information on the computations

including memory and central processing units (CPU) for all cases is given in Table 1.

Results and Discussion

Preliminaries

Before going into details of the presentation of the results, it should be mentioned that the predicted surface pressure is compared with measured data by Kavsaoglu[7] because this study covered a wide region and used very dense pressure taps in the vicinity of the jet nozzles. This can be recognized from figures comparing the finite element mesh and the surface pressure tap locations given in all cases. The point-by-point comparison of the velocity profiles in the circular jet case is also based on the data measured by using a hot-wire anemometer in the same study to give a meaningful comparison. Also, some representative jet properties, including jet axis, axial velocity decay, or vortex curve, are compared with available experimental data. Finally, predicted velocity vector plots on successive xy planes from the wall are given for all cases.

Single Circular Jet in a Crossflow at $R = 4$

The computed trajectory is compared with previous experimental results[4-7] with satisfactory agreement in Fig. 4a. It

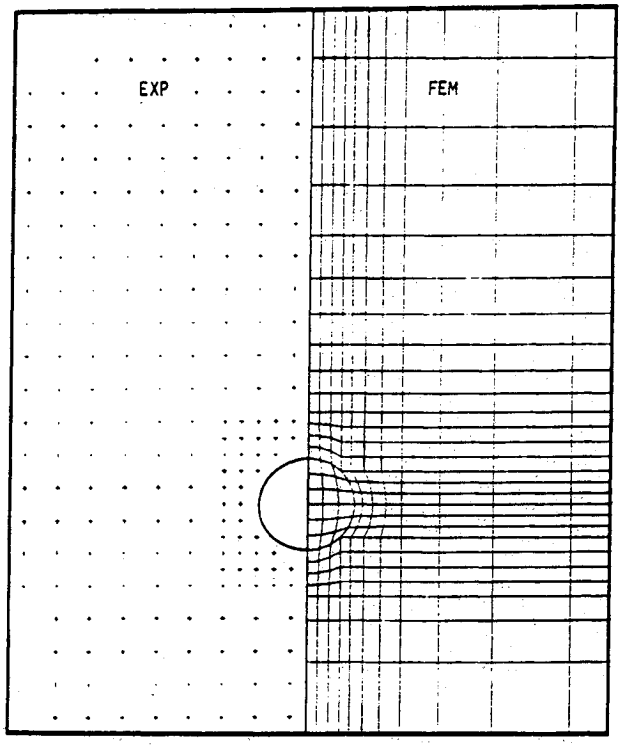

Fig. 5a Wall pressure tap locations vs finite-element mesh.

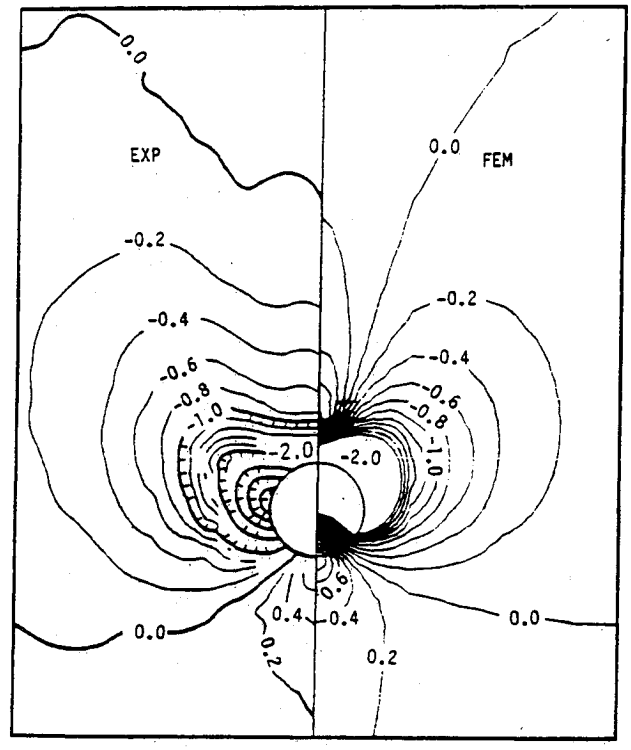

Fig. 5b Comparison of surface pressure coefficient.

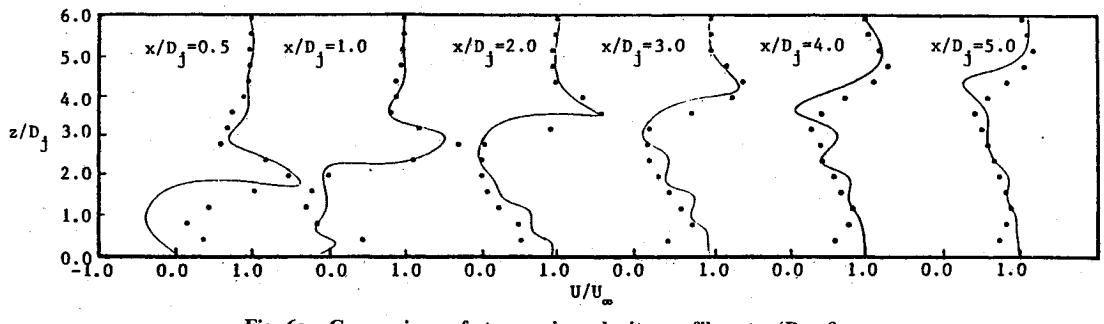

Fig. 6a Comparison of streamwise velocity profiles at $y/D = 0$.

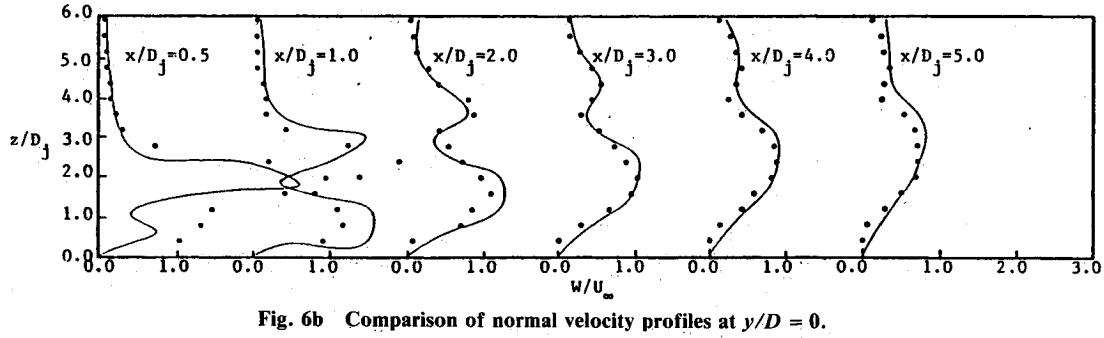

Fig. 6b Comparison of normal velocity profiles at $y/D = 0$.

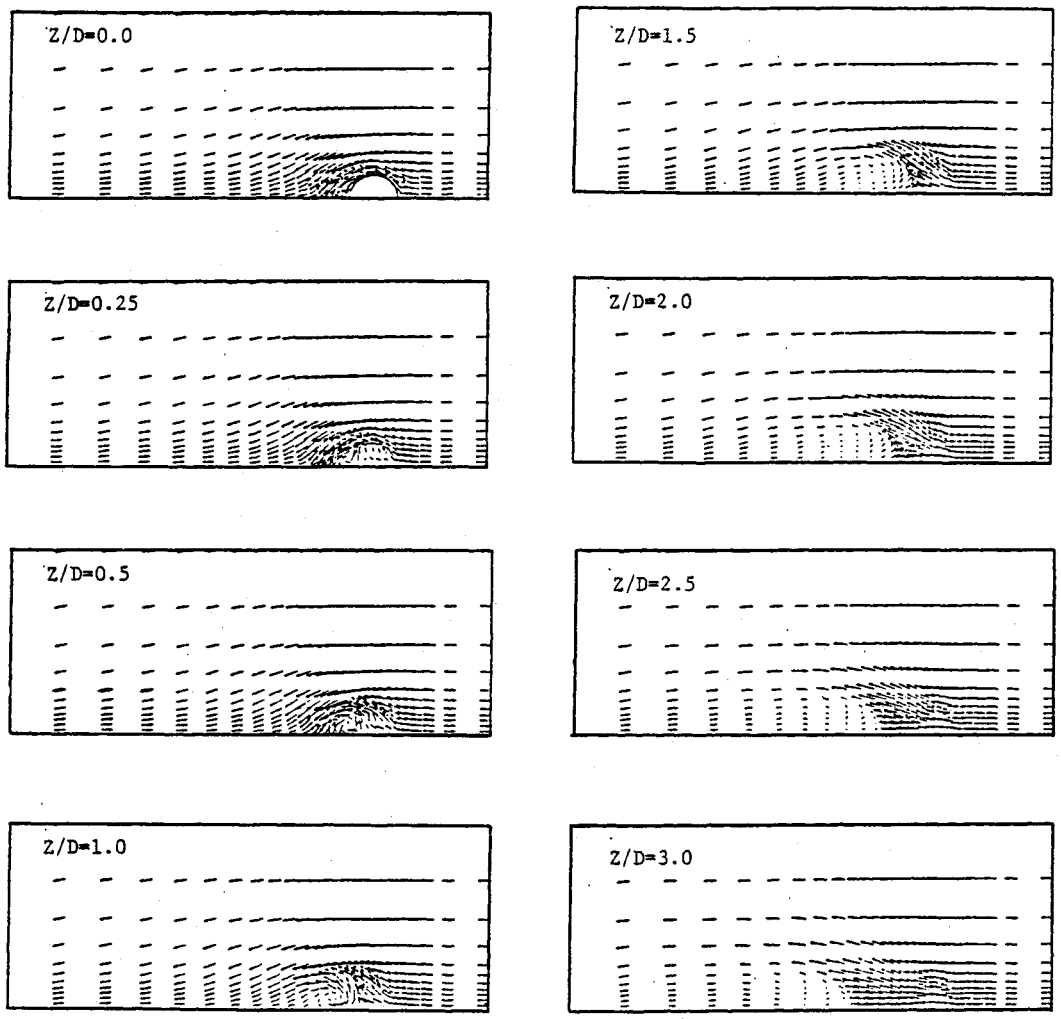

Fig. 7 Display of the velocity vectors on successive *xy* planes.

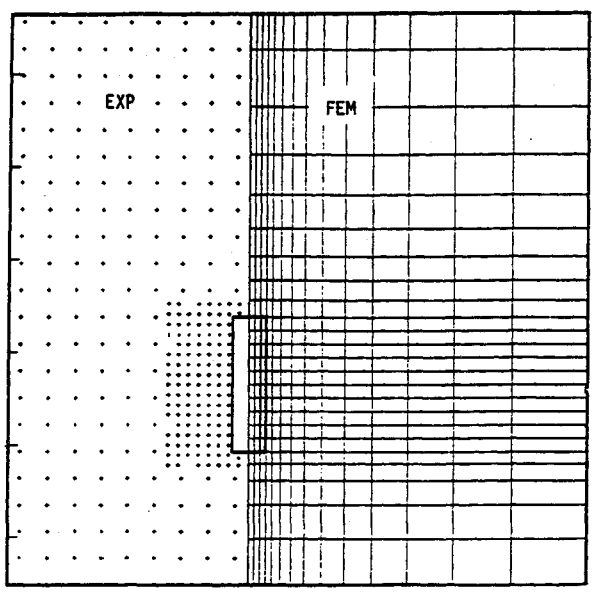

Fig. 8a Wall pressure tap locations vs finite-element mesh.

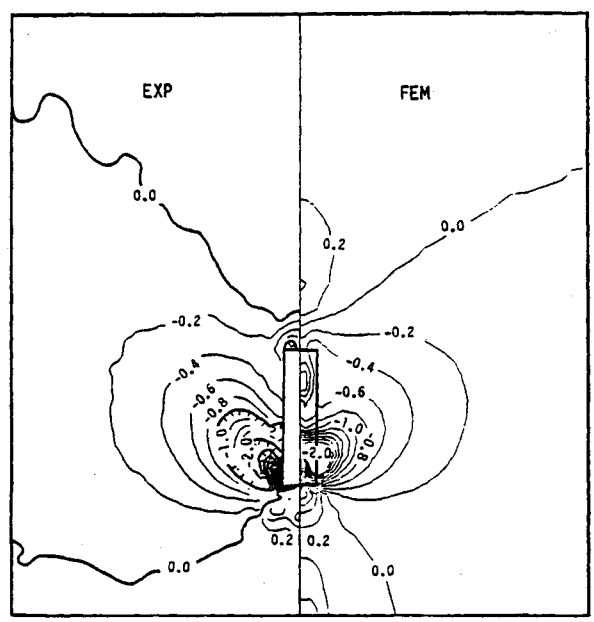

Fig. 8b Comparison of surface pressure coefficient.

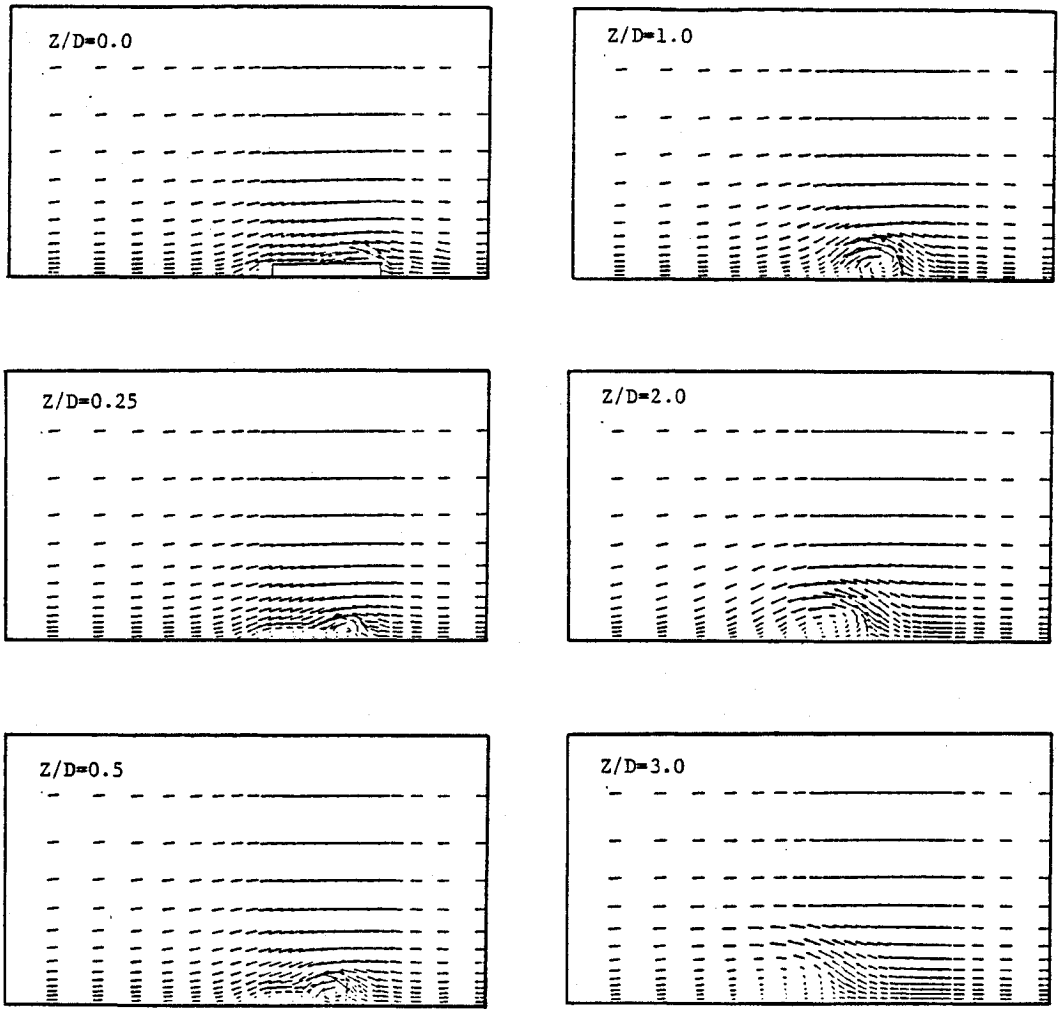

Fig. 9 Display of the velocity vectors on successive *xy* planes.

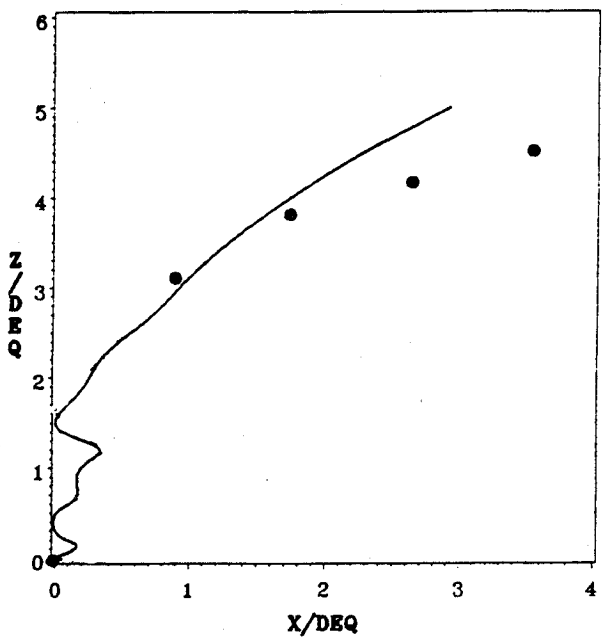

Fig. 10a Comparison of jet trajectory.

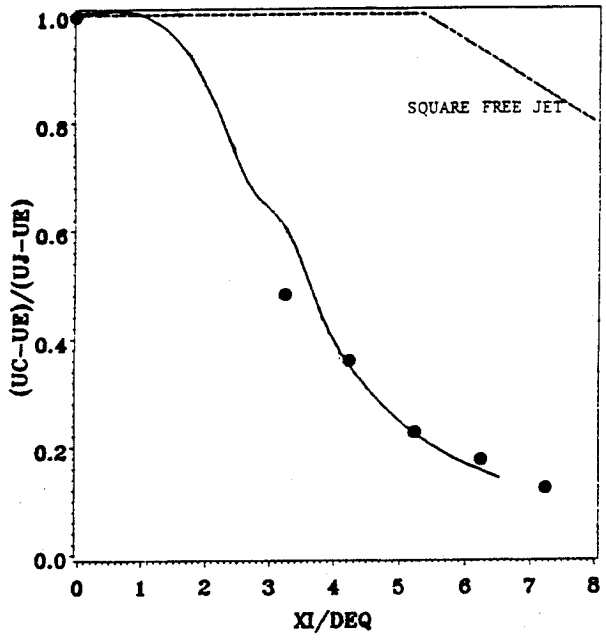

Fig. 10b Comparison of axial velocity decay.

should be noted that even the measured trajectory shows appreciable differences according to the experimental conditions, such as jet exit velocity profile, turbulence level, or crossflow properties. The data of Chassaing et al.[5] indicate a somewhat higher trajectory, whereas the high turbulence case of Kavsaoglu[7] shows a lower trajectory. The computed trajectory appears not to approach the top boundary, and this may be due to the imposition of the traction-free condition on this surface, which specifies zero state of the normal and tangential stress components. The predicted jet shape defined by half-velocity points is compared with the data of Chassaing et al.[5] in Fig. 4b. Even though the prediction shows more deflection, the overall behavior is reasonably reproduced. The axial velocity decay along the arc length of the jet axis is compared with various measured data in Fig. 4c. The prediction shows a slightly faster decay, but it generally compares well with various data. The predicted location of the end of the potential core seems to be near the observed beginning of rapid velocity

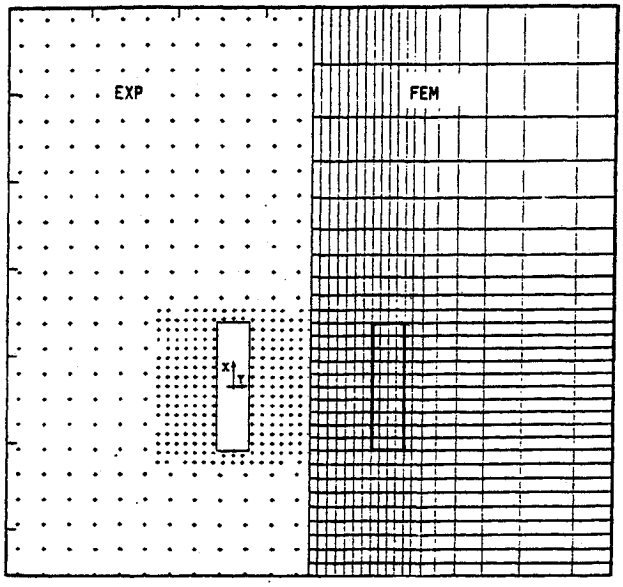

Fig. 11a Wall pressure tap locations vs finite element mesh.

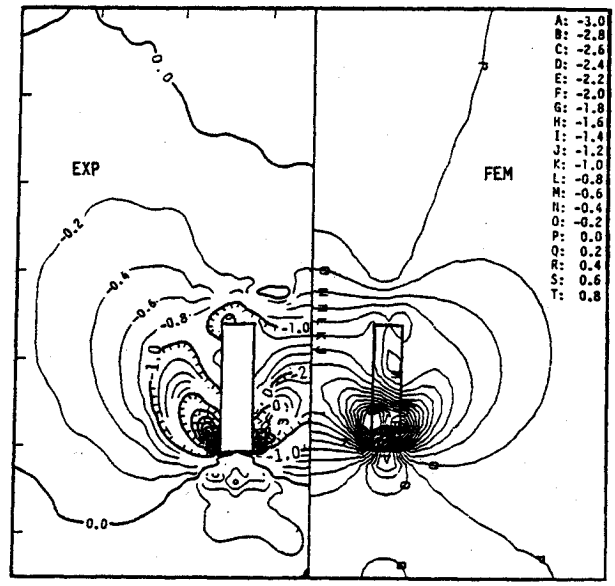

Fig. 11b Comparison of surface pressure coefficient.

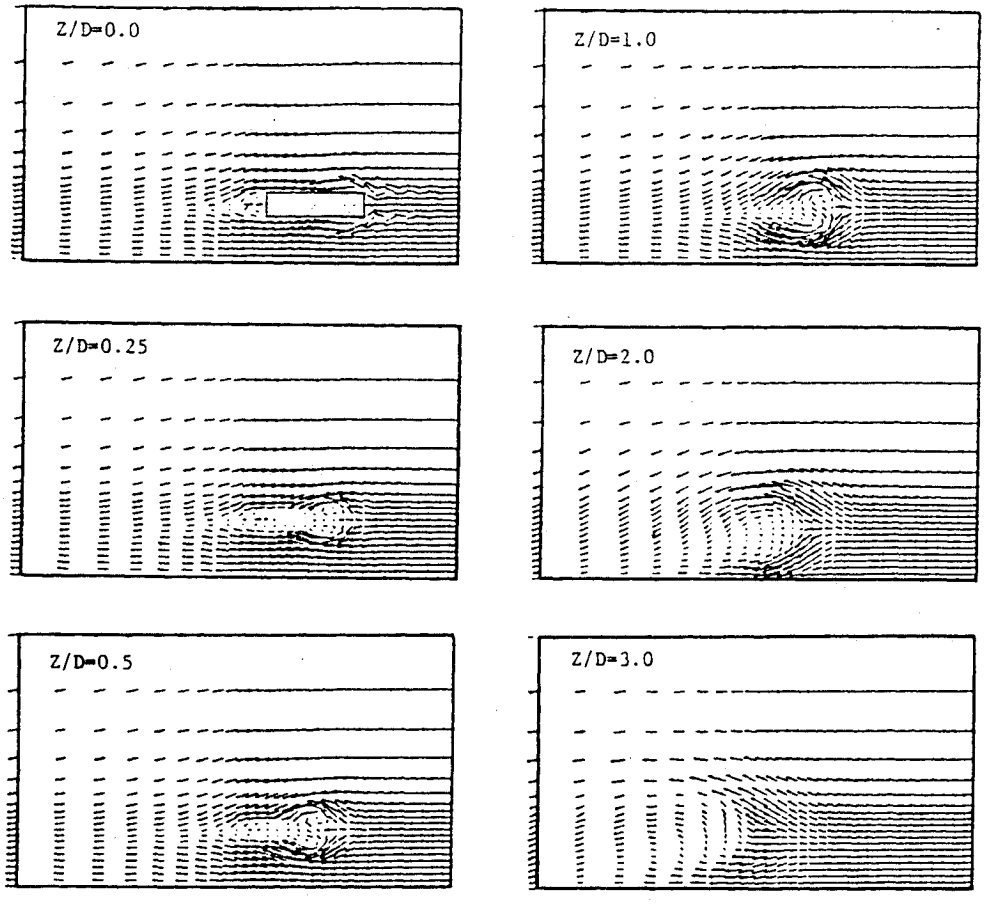

Fig. 12 Display of the velocity vectors on successive *xy* planes.

decay $2<\xi/D<3$. The vortex curve prediction is compared with the measurement,[20] whose data are available from $x/D=2$ in Fig. 4d. The prediction shows better agreement far downstream, and this may be because the computed curve is obtained by determining the vortex center at the yz plane while the measurement of Ref. 20 aligned a rake of probes exactly perpendicular to the vortex axis.

Surface pressure comparison is given in Fig. 5, and the current calculation is shown to predict the important features of the overall pressure pattern quite well, except for the wake region right behind the nozzle. The agreement here is comparable to that achieved by well-tuned, empirical/inviscid flow solutions,[15] and both methods failed to provide an accurate picture in the wake region. This is likely due to the existence of a large separated region downstream of the jet.

Figures 6 shows point-by-point comparison of the mean velocity profiles in the plane symmetry, i.e., xz plane. In Fig. 6a, where the streamwise component is compared, the overall observation is that the use of a slip condition on the wall affected the profiles within 1 jet diam above the wall, but it is not critical for the simulation of main jet flowfield. Importantly, the computation predicts well the location and magnitude of the velocity peaks in spite of the appearance of the wiggle. Figure 6b shows normal velocity comparisons on the same plane, and the agreement downstream of the jet looks excellent. The double peaks of the profile are predicted quite accurately, and the near wall region is also well simulated.

A series of velocity vector plots given in Fig. 7 elucidate the generation and growth of the counter-rotating vortices starting from the wall to 3 jet diam above the wall. It can be easily identified that the vortices are created right behind the nozzle where the negative peak of pressure is observed.

Single Rectangular (Aspect Ratio 4) Jet in a Crossflow at $R = 4$

Because mean velocity data are not available for this case, only the predicted pressure coefficient is compared with the measured data in Fig. 8. The overall pattern is quite well predicted, and the appearance of the negative peaks near the front corner of the nozzle is apparent. The agreement for this presumably more complicated case seems even better than that for the circular jet case, and this may be due to lessened blockage effect and, thereby, a reduced wake zone.

Figure 9 reveals that, unlike the circular jet case, the vortex pair is found to be generated at the front corner of the nozzle. Also, the same is true for the pressure peak.

Dual Rectangular Jets (Side by Side) in a Crossflow at $R = 4$

The trajectory comparison is given in Fig. 10a, which reveals that the calculations show a drift in the initial region and higher penetration in the zone of deflection, but the overall behavior is reasonably predicted. The main reason for the higher penetration may be due to a relatively lower location of the top boundary due to the limitation of computational resources. The axial velocity decay along the jet arc length is compared in Fig. 10b, where the calculation shows good agreement. Measured results for a square free jet are also illustrated for a qualitative comparison, and the present flow shows much faster decay due to the action of the crosswind as in the circular jet case.

Surface pressure comparison in Fig. 11 reveals that the agreement looks excellent. The computed results clearly predict not only the negative peaks at the front corners, but the second negative zone at the rear, which is not so clear in the single rectangular jet case. This difference may be due to jet interaction that locally isolates the region between the nozzles and does not allow a high transverse entrainment velocity.

The velocity patterns given in Fig. 12 indicate the appearance of the asymmetric vortex pairs created at each front corner that lead to the negative peaks of the surface pressure at or near the vortex core region.

Conclusions

Here we have demonstrated reliable and cost-effective numerical techniques to predict the mean flowfield and surface pressure induced by three-dimensional, turbulent jets in a crossflow at R in the range of 4. The present turbulence model was successfully applied to various transverse jet(s) with complex nozzle configurations. According to the comparison of the mean velocity profiles, the entrainment process seems to be reasonably modeled, which in turn results in excellent predictions of the surface pressure distribution. However, for dual jets, further mesh refinement is probably needed for the effect of jet interaction in order to improve the mean flowfield prediction.

Small wiggles are observed in the regions where the velocity gradient is very steep, and this seems to be a natural consequence of using conventional Galerkin-type finite element methods that lead to a centered-difference-like treatment of the advection terms. Even though some error can be attributed to the coarseness of the mesh, since the wiggles are not dominant at essentially all mesh locations and they occur in the regions of lesser importance, the wiggle-free solution in the rest of the mesh is judged of acceptable accuracy. Upwind methods may be useful to suppress the wiggles and to obtain smooth solutions. However, it should be remembered that upwinding is accurate only if the numerical diffusion is significantly less than the physical diffusion, so it can only be used on a very fine mesh. In spite of the presence of the velocity wiggles, no spurious pressure mode was observed because the pressure was computed at the centroid point of the element, which resulted in filtered pressure.

The use of a slip condition on the wall introduces measurable effects on the tangential velocity profiles, but these are limited to the near-wall region. We believe that this approach may be useful if the pressure is the major concern. The use of traction-free conditions on the far-field boundaries is found to handle the mass entrainment or discharge across the boundary effectively with a modest-sized computational region.

Extensions of the current work may include dual jets injected from a flat surface in tandem configurations and jets injected from a body of revolution. Previous crude techniques for tandem jets with inviscid methods simply treat each jet as a single jet and use the jet properties correlated for injection from a flat surface until both merge into one. Jet-to-jet spacing is another key parameter, and the turbulent mixing will surely be different from that of single jet cases or widely spread jets. Similar techniques can be used for the body of revolution case, where the jet-to-body diameter ratio varies from a very small value[23] to about one-half.[16] Also, the change of other properties of the jet and crossflow, such as nonuniform jet exit profile, swirl, turbulence, temperature differences, injection angle, and nonuniform crossflow profiles, may be included.

Appendix A: Development of the Algebraic Turbulence Function Hypothesis

Using the unified eddy-viscosity model[1] (or any Prandtl-type model) for the planar-free shear flow, the turbulent shear stress may be given as

$$\frac{\tau_T}{\rho} = -\overline{u'v'} = C\frac{\Delta U_C}{b}\int_0^\infty \Delta U\,dy \simeq C \times C_1(\Delta U_C)^2 \qquad \text{(A1)}$$

where C_1 is a constant that depends on the specific profile shape, and typical shapes yield a value of roughly one-half. On the other hand, one may write[35]

$$-\overline{u'v'} = C_2\sqrt{\overline{u'^2}}\sqrt{\overline{v'^2}} \qquad \text{(A2)}$$

where C_2 is also a constant of about one-half. Also, generally in free shear flows, the following can be conjectured[35]

$$u' = v' \qquad \text{(A3)}$$

Thus, the final result may be written as

$$\bar{u}'^2/(\Delta U_c)^2 \simeq C \qquad \text{(A4)}$$

because C_1/C_2 is expected to be near unity. In other words, once the axial turbulent intensity information is given, an eddy-viscosity model applied to a specific free shear flow can be applied to the other cases if the proportionality constant is adjusted.

References

[1]Schetz, J. A., *Injection and Mixing in Turbulent Flow,* Progress in Astronautics and Aeronautics, Vol. 68, AIAA, New York, 1980.

[2]Abramovich, G. N., *The Theory of Turbulent Jets,* MIT, Cambridge, MA, 1960.

[3]Keffer, J. F., and Baines, W. D., "The Round Turbulent Jet in a Cross Wind," *Journal of Fluid Mechanics,* Vol. 15, Pt. 4, 1963, pp. 481–497.

[4]Kamotani, Y., and Greber, I., "Experiments on a Turbulent Jet in Cross-Flow," *AIAA Journal,* Vol. 10, No. 11, 1972, pp. 1425–1429.

[5]Chassaing, P., George, J., Claria, A., and Sananes, F., "Physical Characteristics of Subsonic Jets in a Cross-Stream," *Journal of Fluid Mechanics,* Vol. 62, Pt. 1, 1974, pp. 41–64.

[6]Jordinson, R., "Flow in a Jet Directed Normal to the Wind," Aeronautical Research Council, London, R&M 3074, 1956.

[7]Kavsaoglu, M., "Jets in a Crossflow Including the Effect of Dual Arrangements, Angle, Shape, Swirl, and High Turbulence," Ph.D. Dissertation, Virginia Polytechnic Institute and State Univ., VA, Dec. 1986.

[8]Chien, C. J., and Schetz, J. A., "Numerical Solution of Three-Dimensional Navier-Stokes Equations with Applications to Channel Flows and a Buoyant Jet in a Cross-Flow," *Journal of Applied Mechanics*, Vol. 42, Sept. 1975, pp. 575–579.

[9]Patankar, S. V., Basu, D. K., and Alpay, S. A., "Prediction of the Three Dimensional Velocity Field of a Deflected Turbulent Jet," *Journal of Fluids Engineering,* Vol. 99, No. 4, 1977, pp. 758–762.

[10]White, A. J., "The Prediction of the Flow and Heat Transfer in the Vicinity of the Jet in Cross Flow," American Society of Mechanical Engineers, ASME-80-WA/HT-26, 1980.

[11]Sykes, R. I., Lewellen, W. S., and Parker, S. F., "On the Vorticity Dynamics of a Turbulent Jet in a Crossflow," *Journal of Fluid Mechanics,* Vol. 168, 1986, pp. 393–413.

[12]Baker, A. J., Snyder, P. K., and Orzechowski, J. A., "Three Dimensional Nearfield Characterization of a VSTOL Jet in Turbulent Crossflow," AIAA Paper 87-0051, Jan. 1987.

[13]Mongia, H. C., Reynolds, R. S., and Srinivasan, R., "Multidimensional Gas Turbine Combustion Modeling: Applications and Limitations," *AIAA Journal,* Vol. 24, No. 6, 1986, pp. 890–904.

[14]Holdeman, J. D., and Srinivasan, R., "Modeling Dilution Jet Flowfields," *Journal of Propulsion and Power,* Vol. 2, No. 1, 1986, pp. 4–10.

[15]"Analysis of a Jet in a Subsonic Crosswind," NASA SP-218, 1969.

[16] Schetz, J. A., Jakubowski, A. K., and Aoyagi, K., "Jet Trajectories and Surface Pressures Induced on a Body of Revolution with Various Dual Jet Configurations," *Journal of Aircraft,* Vol. 20, No. 11, 1983, pp. 975–982.

[17]Schetz, J. A., Jakubowski, A. K., and Aoyagi, K., "Surface Pressures Induced on a Flat Plate with In-Line and Side-by-Side Dual Jet Configurations," *Journal of Aircraft,* Vol. 21, No. 7, 1984, pp. 484–490.

[18]Moore, C. L., and Schetz, J. A., "Effects of Nonuniform Velocity Profiles on Dual Jets in a Crossflow," AIAA Paper 85-1674, July 1985.

[19]Kavsaoglu, M., Schetz, J. A., and Jakubowski, A. K., "Dual Rectangular Jets from a Flat Plate in a Crossflow," AIAA Paper 86-0477, Jan. 1986.

[20]Weston, R. P., and Thames, F. C., "Properties of Aspect Ratio 4.0 Rectangular Jets in a Subsonic Crossflow," *Journal of Aircraft,* Vol. 16, No. 10, 1979, pp. 701–707.

[21]Kuhlman, J. M., Ousterhout, D. S., and Warcup, R. W., "Experimental Investigation of Effect of Jet Decay Rate on Jet-Induced Pressures on a Flat Plate," NASA CR-2979, 1978.

[22]Kuhlman, J. M., Ousterhout, D. S., and Warcup, R. W., "Experimental Investigation of Effects of Jet Decay Rate on Jet-Induced Pressures on a Flat Plate: Tabulated Data," NASA CR-158990, 1978.

[23]Ousterhout, D. S., "An Experimental Investigation of a Cold Jet Emitting from a Body of Revolution into a Subsonic Free Stream," NASA CR-2089, 1972.

[24]Sani, R. L., Gresho, P. M., Lee, R. L., Griffiths, D. F., and Engelman, M. S., "The Cause and Cure(?) of the Spurious Pressures Generated by Certain FEM Solutions of the Incompressible Navier-Stokes Equations: Part 2," *International Journal for Numerical Methods in Fluids,* Vol. 1, 1981, pp. 171–204.

[25]Engelman, M. S., Sani, R. L., Gresho, P. M., and Bercovier, M., "Consistent vs Reduced Integration Penalty Methods for Incompressible Media Using Several Old and New Elements," *International Journal for Numerical Methods in Fluids,* Vol. 2, 1982, pp. 25–42.

[26]Reddy, J. N., "On the Penalty Function Methods in the Finite Element Analysis of Flow Problems," *International Journal for Numerical Methods in Fluids,* Vol. 2, 1982, pp. 151–171.

[27]Oh, T. S., "Navier-Stokes Prediction of the Three Dimensional Flowfield of Jets in a Crossflow Using the Finite Element Method," Ph.D. Dissertation, Virginia Polytechnic Institute and State Univ., VA, March 1988.

[28]Bradshaw, P., Cebeci, T., and Whitelaw, J. H., *Engineering Calculation Methods for Turbulent Flow,* Academic, 1981.

[29]Crabb, D., Durao, D. F. G., Whitelaw, J. H., "A Round Jet Normal to a Crossflow," *Journal of Fluids Engineering,* Vol. 103, 1981, pp. 142–153.

[30]Andreopoulos, J., and Rodi, W., "Experimental Investigation of Jets in a Crossflow," *Journal of Fluid Mechanics,* Vol. 138, 1984, pp. 93–127.

[31]"Free Turbulent Shear Flows," NASA SP-321, 1973.

[32]Sforza, P. M., Steiger, M. H., and Trentacoste, N., "Studies on Three-Dimensional Viscous Jets," *AIAA Journal,* Vol. 4, No. 5, 1966, pp. 800–806.

[33]Pratte, B. D., and Baines, W. D., "Profiles of the Round Turbulent Jet in a Cross Flow," *Proceedings of ASCE, Journal of the Hydraulics Division,* Vol. 93, Nov. 1967, pp. 56–63.

[34]Schetz, J. A., "Some Studies of the Turbulent Wake Problem," *Astronautics Acta,* Vol. 16, No. 2, 1971, pp. 107–117.

[35]Schlichting, H., *Boundary Layer Theory,* 7th ed. McGraw-Hill, 1979.

[36]Roache, P. J., *Computational Fluid Dynamics,* Hermosa, 1976.

[37]Engelman, M. S., "FIDAP: A Fluid Dynamic Analysis Program," *Advances in Engineering Software,* Vol. 4, 1982.

[38]Gresho, P. M., and Lee, R. L., "Don't Suppress the Wiggles—They're Telling You Something," *Computer and Fluids,* Vol. 9, 1981, pp. 223–253.